

# Simplified equations for Vierendeel design calculations of composite beams with web openings

Pattamad Panedpojaman\*

Department of Civil Engineering, Faculty of Engineering, Prince of Songkla University, Songkhla 90110, Thailand

(Received July 13, 2017, Revised December 9, 2017, Accepted March 17, 2018)

**Abstract.** Composite beams with web openings are vulnerable to Vierendeel bending failure. The available methods provide quite conservative estimates of Vierendeel bending resistance. An alternative design method to compute the resistance was proposed in this study, based on quadratic nonlinear interactions of normalized shear force, axial force and Vierendeel bending moment. The interactions of the top and bottom Tee section must satisfy mutual conditions to prevent the Vierendeel failure. The normalized shear force and Vierendeel bending moment of the composite part were used instead in the top Tee interaction. The top Tee axial force was computed based on force equilibrium. Based on a rigid-plastic model, the composite resistance is estimated using an effective slab width of the vertical shear resistance. On using the proposed method, nonlinear reductions due to shear loads and axial forces are not required, in contrast to prior methods. The proposed method was validated against experiments from literature. The method limitations and accuracy as well as the Vierendeel behavior were investigated by finite element simulations, with varied composite beam parameters. The proposed design loads are less conservative than earlier estimates and deviate less from the simulations.

**Keywords:** design; Vierendeel failure; composite beam; web opening; co-existing action

## 1. Introduction

For composite floor systems or composite beams, the composite action is developed using shear studs welded on top of steel beams embedded in concrete slabs. The composite beams are commonly used in commercial buildings. In order to minimize the overall height of the building, it is necessary to have large web openings in the beams for passing through piping or wiring. However, the web openings weaken the beams, causing concerns of structural failure, such as shear failure, flexural failure, and Vierendeel bending failure around the opening. Various design approaches for cellular beam and composite beams with web openings (Chung and Lawson 2001, Chung *et al.* 2005, Durif *et al.* 2015, Erdal 2015, 2016, Kataoka *et al.* 2017, Lawson 2011, Serror *et al.* 2016, Ward 1990) have been proposed. Load capacity of the system depends on many factors, such as opening sizes, opening shapes, opening or load locations, section properties of steel beams, and composite behavior.

Vierendeel bending is focused in this study. The shear forces transferred through perforated steel section cause secondary moments (Vierendeel bending moments) in sections above and below the web opening. The Vierendeel mechanism is interactions of the secondary moments with the shear force and the global bending moment. Generally, in non-composite beams, the Vierendeel bending is resisted by plastic bending of the steel web-flange Tee sections at

the four corners of the web opening. In composite beams, the local composite resistance of the top Tee section and the concrete slab also resists Vierendeel bending. The composite behavior depends on shear force transfer, pull-out events and concrete crushing in the slab (Lawson *et al.* 2013). Therefore, two contributions to the resistance must be considered: the plastic bending of the Tee sections and the composite action.

For the plastic bending of the Tee sections, SCI P100 (Ward 1990) evaluated the Vierendeel bending resistance through linear interaction of the moment ratio and the local axial ratio occurred in the Tees. Lawson *et al.* (2006, 2013) and SCI P355 (Lawson 2011) considered a net Vierendeel bending resistance after effects of the shear load and the global moment on the Tees. A nonlinear reduction of web thickness to account for the shear load and the global moment is required in these methods (Ward 1990, Lawson 2011, Lawson *et al.* 2013). The methods provide quite conservative estimates of the Vierendeel bending resistance (Panedpojaman *et al.* 2015). In terms of section moment-shear-interactions, numerical simulations of steel beams with web openings have been used to investigate the Vierendeel bending resistance (Liu and Chung 2003). The moment-shear-interaction curve is adjusted by using Vierendeel coefficients based on empirical studies. Therefore, the interaction method is limited to predetermined geometries of perforated steel beams. Based on a quadratic nonlinear failure criterion of the normalized global moment, shear load and Vierendeel bending, an alternative design method was proposed to check for the Vierendeel failure (Panedpojaman *et al.* 2015). Compared with other available methods in literature, the method in

\*Corresponding author, Ph.D., Associate Professor,  
E-mail: [ppattamad@eng.psu.ac.th](mailto:ppattamad@eng.psu.ac.th)

Panedpojaman *et al.* (2015) is more accurate and simpler for the Vierendeel bending check without the web thickness reduction. However, only non-composite symmetric perforated beams are the limit of the method.

To resist Vierendeel bending, many assumptions about the composite action for a composite beam with a web opening have been proposed (Chung and Lawson 2001, Chung *et al.* 2005, Lawson *et al.* 2006, Lawson 2011, Ward 1990). As an example, under global moment and shear force, Chung *et al.* (2005) considered local forces such as shear forces and axial forces occurred in the top composite part and the steel Tee section below the web opening. The Vierendeel bending resistance of the composite action is generated by the different moment arms between the axial forces, acting on the top composite part and the section below the web opening, at the low moment side and the high moment side of the openings. Note that the axial forces are the same in the two sides. Lawson *et al.* (2006) and SCI P355 (Lawson 2011) considered that the different axial forces in the low moment side and the high moment side generates the Vierendeel bending resistance whereas the moment arms on the two sides are approximately equal. The force difference equals the longitudinal shear force resisted by each shear stud along the opening length.

SCI P355 method is well-known and practical in the design for Vierendeel bending resistance. However, the Vierendeel bending resistance computed by using SCI P355 is significantly conservative in some cases, especially with a long opening. Furthermore, the method does not directly consider effects of concrete thickness or concrete crushing behavior of the slab. In order to comprehend the failure mechanism by pull-out of the shear stud, behavior of the shear studs along the opening is presented in terms of a rigid-plastic mechanism (Lawson *et al.* 2013). The mechanism considers the work done in concrete crushing by the slab. The mechanism problems are solved based on the minimum energy solution. However, the Vierendeel bending resistance obtained from the rigid-plastic mechanism is in many cases an overestimate.

Since these available methods have the limitations, this study aims to develop a simple and effective design method for the Vierendeel bending resistance of composite beams with web openings. The proposed method is derived based on the quadratic nonlinear failure criterion and the rigid-plastic mechanism. Through a parametric study using finite element analysis, the Vierendeel behavior and limitations of the proposed method are also investigated. The study focused on composite beams with rectangular, circular and elongated openings. Note that shapes of hexagonal openings can also affect Vierendeel bending resistance. Therefore, to limit the parameters in the parametric study, composite beams with hexagonal openings are not included in this investigation.

## 2. Vierendeel mechanism and design

Vierendeel bending moment  $MV$  is a consequence of shear forces transferred through a perforated steel section with an effective length of openings. To design a steel beam with a web opening, the Vierendeel bending moment must

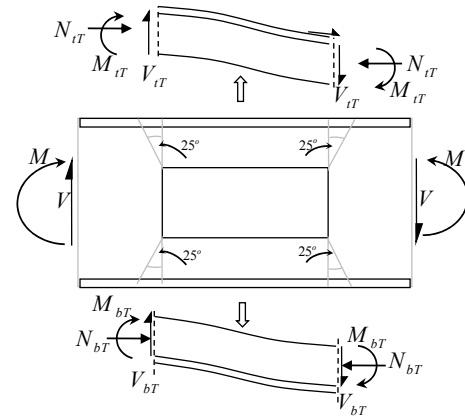


Fig. 1 Vierendeel mechanism in a steel beam with a rectangular web opening

be less than its Vierendeel bending resistance. Consider a non-composite steel beam with a rectangular opening, under the global bending moment  $M$ , the shear force  $V$  and Vierendeel bending moment  $MV$  as shown in Fig. 1. Effects of the global bending moment and the shear force may degrade the Vierendeel bending resistance. An effective web thickness has been used in the literature (Chung *et al.* 2005, Lawson *et al.* 2006, Lawson 2011, Lawson *et al.* 2013) to decrease the Vierendeel bending resistance. A shortcut to estimating the effective web thickness, namely the quadratic nonlinear failure criterion (Panedpojaman *et al.* 2015), is applied in this study. Key concepts of the proposed method based on the quadratic nonlinear failure criterion are presented in Section 2.1. Furthermore, a Vierendeel bending resistance of the composite action is proposed to reformulate in Section 2.2. Mainly based on Eurocodes and SCI P355, Sections 2.3-2.5 briefly describe computations of other parameters required in the proposed method.

### 2.1 Force interaction in Tees

Normalized moment-shear-Vierendeel bending interactions through a quadratic Panedpojaman *et al.* (2015) for non-composite symmetric steel beams. The interacting shear force  $V$ , moment  $M$  and Vierendeel bending moment  $MV$  in Eq. (1) must jointly satisfy.

$$\left(\frac{V}{V_{o,rd}}\right)^2 + \left(\frac{M}{M_{o,rd}}\right)^2 + \left(\frac{MV}{MV_{o,rd}}\right)^2 \leq 1 \quad (1)$$

where  $V_{o,rd}$  is the shear resistance of the perforated section,  $M_{o,rd}$  is the moment resistance of the perforated section, and  $MV_{o,rd}$  is the Vierendeel bending resistance of the perforated section. Since the axial force  $N$  corresponds to the moment  $M$ , the axial force utilization  $N / N_{T,rd}$  can be substituted for the moment utilization  $M / M_{o,o}$  as in Eq. (2).

$$\left(\frac{V}{V_{o,rd}}\right)^2 + \left(\frac{N}{N_{T,rd}}\right)^2 + \left(\frac{MV}{MV_{o,rd}}\right)^2 \leq 1 \quad (2)$$

With the criterion in Eqs. (1) or (2), no web thickness

reduction is required in the computation. Note that the shear force, moment and Vierendeel moment are equally shared between the top and bottom Tee sections. Therefore, the resistances of the overall perforated section can be used in the equations.

For a non-composite or composite asymmetric steel beam, all forces are not equal at the top and at the bottom. Therefore, Eqs. (1) and (2) proposed in Panedpojaman *et al.* (2015) cannot be applied to. The shear load and Vierendeel bending moment are distributed over three parts, the bottom part, the top part and the concrete slab as in Eqs. (3) and (4), respectively.

$$V = V_{bT} + V_{iT} + V_c \quad (3)$$

$$MV = MV_{bT} + MV_{iT} + MV_c = (V_{bT} + V_{iT} + V_c)l_{eff} \quad (4)$$

where the subscripts *T*, *iT*, *bT* and *c* refer to the Tee section, the top Tee section, the bottom Tee section and the concrete slab, respectively, and  $l_{eff}$  is the effective moment arm to compute Vierendeel moment. For a regular opening,  $l_{eff}$  is the opening width  $l_o$ . Note that  $MV = Vl_{eff}$ .

Consider a non-composite asymmetric steel beam as shown in Fig. 1. Since the forces are not equal at the top and at the bottom, this study proposed that the interactions must be separately assessed for the bottom part and the top part, as in Eqs. (5) and (6).

$$\left(\frac{V_{bT}}{V_{bT,rd}}\right)^2 + \left(\frac{N_{bT}}{N_{bT,rd}}\right)^2 + \left(\frac{MV_{bT}}{MV_{bT,rd}}\right)^2 \leq 1 \quad (5)$$

$$\left(\frac{V_{iT}}{V_{iT,rd}}\right)^2 + \left(\frac{N_{iT}}{N_{iT,rd}}\right)^2 + \left(\frac{MV_{iT}}{MV_{iT,rd}}\right)^2 \leq 1 \quad (6)$$

The subscript *rd* refers to the force resistance. To design an asymmetric steel beam, the forces and Vierendeel bending moment must satisfy both these equations.

In cases of a composite asymmetric steel beam as shown in Fig. 2, the composite action takes place in the top Tee section. This study assumes that the shear load and Vierendeel bending are distributed based on its resistances. Therefore, ratio of the shear load and Vierendeel bending to its resistance is the same in the top Tee section, the concrete slab, and the composite part, as described in Eqs. (7) and (8).

$$\frac{V_{iT}}{V_{iT,rd}} = \frac{V_c}{V_{c,rd}} = \frac{V_{iT} + V_c}{V_{iT,rd} + V_{c,rd}} = \frac{V_{ctT}}{V_{ctT,rd}} \quad (7)$$

$$\frac{MV_{iT}}{MV_{iT,rd}} = \frac{MV_c}{MV_{c,rd}} = \frac{MV_{iT} + MV_c}{MV_{iT,rd} + MV_{c,rd}} = \frac{MV_{ctT}}{MV_{ctT,rd}} \quad (8)$$

where  $V_{ctT}$  and  $MV_{ctT}$  are the shear force and Vierendeel bending moment resisted by the steel top Tee section and the concrete slab, i.e., the composite part, and  $V_{ctT,rd}$  and  $MV_{ctT,rd}$  are the shear and Vierendeel bending resistances of the composite part. Computations of the Vierendeel bending

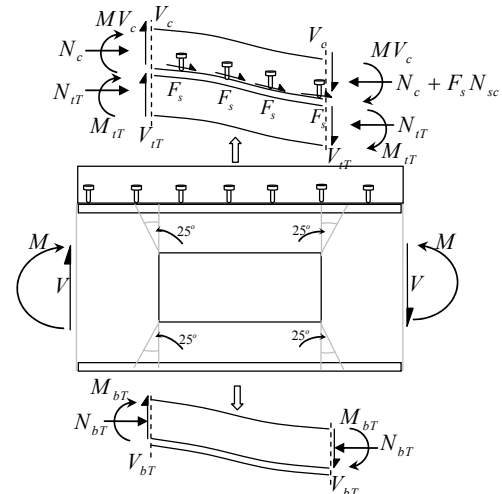


Fig. 2 Vierendeel bending resistance for a composite beam with a rectangular web opening

resistance and the shear resistance are described in Section 2.2 and 2.3, respectively. By substituting Eqs. (7) and (8) into Eq. (6), the interaction of the composite part can be represented as

$$\left(\frac{V_{ctT}}{V_{ctT,rd}}\right)^2 + \left(\frac{N_{iT}}{N_{iT,rd}}\right)^2 + \left(\frac{MV_{ctT}}{MV_{ctT,rd}}\right)^2 \leq 1 \quad (9)$$

To resist the axial compression force caused by the global moment, the concrete slab supports the top Tee section, on the condition that the shear studs have enough shear load carrying capacity. The slab, as an extreme layer, mainly resists the compressive force from the moment (Lawson 2011). The compressive force which surpasses the axial force resistance of the concrete slab is resisted by the steel top part. Therefore, the concept of load distribution based on resistances cannot be applied to the axial force. Computations on  $N_{iT}$  and  $N_{iT,rd}$  are described in Section 2.4.

## 2.2 Vierendeel bending resistance for rectangular openings

For a composite beam with web openings, the Vierendeel bending resistance is the combined bending resistance of the Tee sections above and below the opening at the four opening corners,  $MV_{T,rd}$ , and the concrete resistance,  $MV_{c,rd}$ . The Vierendeel bending resistance of the bottom part or the top part (two opening corners) in Eq. (10) is approximately computed based on the plastic moment resistance of the critical Tee section at 25° from the vertical centerline (Panedpojaman *et al.* 2015).

$$MV_{T,rd} = 2(1.17M_{T,rd}) \quad (10)$$

where  $M_{T,rd}$  is the bending resistance at the vertical centerline of opening corner. The plastic moment resistance of the vertical Tee section is used for the compact section according to BS EN 1993-1-1 (2005). As shown in Fig. 2, the Vierendeel bending resistances of the composite top

part,  $MV_{ct,rd}$ , is the Vierendeel bending resistance of the top part (two opening corners) and the concrete resistance as in Eq. (11). Note that  $MV_{ct,rd}$  is determined by interaction between the shear stud and the concrete slab.

$$MV_{ct,rd} = 2(1.17M_{tT,rd}) + MV_{c,rd} \quad (11)$$

To improve the accuracy of the predicted concrete resistance  $MV_{c,rd}$ , Lawson *et al.* (2013) proposed a rigid-plastic model. The model's Vierendeel bending resistance was represented as the maximum shear force,  $V_{c,RP}$ , at the pull-out failure, and crushing of the concrete slab in Eq. (12).

$$V_{c,RP} = \frac{P_{rd}}{s_s} (h_p + 0.5h_c) \left[ 1 - \frac{P_{rd}}{2P_{v,rd}} \frac{(h_p + 0.5h_c)}{l_o} \right] + 0.25f_c h_c^2 \frac{b_{eff}}{l_o} \quad (12)$$

where  $P_{rd}$  is the shear resistance of the shear stud,  $s_s$  is the spacing of the shear stud,  $h_p$  is the depth of the deck profile,  $h_c$  is the depth of concrete above the deck profile,  $P_{v,rd}$  is the pull-out resistance of the shear stud,  $f_c$  is the compressive strength of concrete, and  $b_{eff}$  is the effective slab width.

In the equation, effects of the pull-out and shear resistance of the shear stud, and the concrete crushing are represented in the first and second term, respectively. The model also considers effects of the low moment side of a perforated section in a composite steel beam. A part of the concrete slab at the low moment side is in tension and affects the composite action. Further details and derivations of Eq. (12) are available in Lawson *et al.* (2013). In this study, the maximum shear force is converted to the Vierendeel bending resistance in Eq. (13) by multiplying with the moment arm of Vierendeel bending, namely the opening length  $l_o$ .

$$MV_{c,rd} = \frac{P_{rd}}{s_s} (h_p + 0.5h_c) \left[ l_o - \frac{P_{rd}}{2P_{v,rd}} (h_p + 0.5h_c) \right] + 0.25f_c h_c^2 b_{eff} \quad (13)$$

However, relative to the Vierendeel bending resistances estimated from finite element models in the parametric study of this paper, the overestimate results of the rigid-plastic model in Eq. (13) are clearly observed. Therefore, the composite resistance,  $MV_{c,rd}$ , is in need to reformulate.

To compute the Vierendeel bending resistance from concrete crushing of the rigid-plastic model, Lawson *et al.* (2013) used the effective slab width  $b_{eff}$ , which is the slab width affected by compressive forces due to the global moment. Such effective slab width is used on computing compression resistance of the concrete slab. However, based on the parametric study and stress observed in finite element models of this study, the Vierendeel bending resistance closely relates to the vertical shear resistance of the concrete slab, not the bending action. Therefore, an appropriate effective slab width should be relevant to the

shear resistance of the concrete slab. In other words, the concrete slab crushing that affects the Vierendeel bending resistance should be scoped in the shear zone. The effective slab width of the compressive resistance,  $b_{eff}$ , in Eq. (14) and the vertical shear resistance,  $b_w$ , in Eq. (15) are specified in SCI P355 as follows

$$b_{eff} = 3L/16 + x/4 \quad \text{for} \quad x \leq L/4 \quad (14)$$

$$b_{eff} = L/4 \quad b_{eff} = L/4 \quad \text{for} \quad x > L/4$$

$$b_w = b_f + 2h_{s,eff} \quad (15)$$

where  $h_{s,eff}$  is the effective depth of slab for punching shear approximated as  $0.75h_s$ , and  $h_s$  is the slab depth. Effects of  $b_{eff}$  and  $b_w$  on the computation of the Vierendeel bending resistance describes in the last paragraph of Section 4.2.1.

Under Vierendeel bending, the longitudinal shear force and the pull-out force simultaneously act on the shear stud. These forces generally affect each other's resistance (Wang and Chung 2008). However, to simply compute the Vierendeel bending resistance, the pull-out resistance  $P_{v,rd}$  is taken as half of the shear resistance,  $P_{rd}/2$  (Lawson *et al.* 2013, Wang and Chung 2008). By substituting  $b_{eff}$  with  $b_w$  and substituting  $P_{v,rd}$  with  $P_{rd}/2$  in Eq. (13), the Vierendeel bending resistance is reformulated in Eq. (16).

$$MV_{c,rd} = \frac{P_{rd}}{s_s} \left[ (h_p + 0.5h_c) l_o - (h_p + 0.5h_c)^2 \right] + 0.25f_c h_c^2 b_w \quad (16)$$

Note that based on the parametric study of this paper, the second term in Eq. (16) must be neglected when the distance from the nearest support to the opening centerline,  $l_{so}$ , is less than 1.5 times the opening length,  $l_{so} < 1.5l_o$ . Since the pull-out force of the shear studs along the distance is not enough to restrain the concrete slab in place, concrete crushing cannot be completed.

### 2.3 Shear resistance

The characteristic shear resistance of the Tee sections,  $V_{T,rd}$ , is given by Eq. (17) according to BS EN 1993-1-1 (2005). The shear area of the Tee sections is consisting of the web area and some portions of the flange. For reinforced concrete members without shear reinforcement, BS EN 1992-1-1 (2004) gives the minimum shear resistance  $V_{c,rd}$  as in Eq. (18)-(20). Further design details can be studied from the codes.

$$V_{T,rd} = 0.577f_y A_{v,T} \quad (17)$$

$$V_{c,rd} = (0.035k^{3/2} f_c^{1/2} + 0.15\sigma_{cp}) b_w h_c \quad (18)$$

$$k = 1 + \sqrt{200/h_c} \leq 2 \quad (19)$$

$$\sigma_{cp} = N_c / (b_{eff} h_c) \quad (20)$$

where  $f_y$  is the yield stress of the steel,  $A_{v,T}$  is the shear area of the Tee section,  $\sigma_{cp}$  is the compressive stress in the concrete slab, and  $N_c$  is the compressive force in the concrete slab.

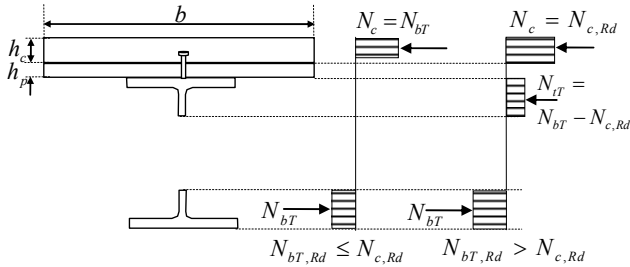
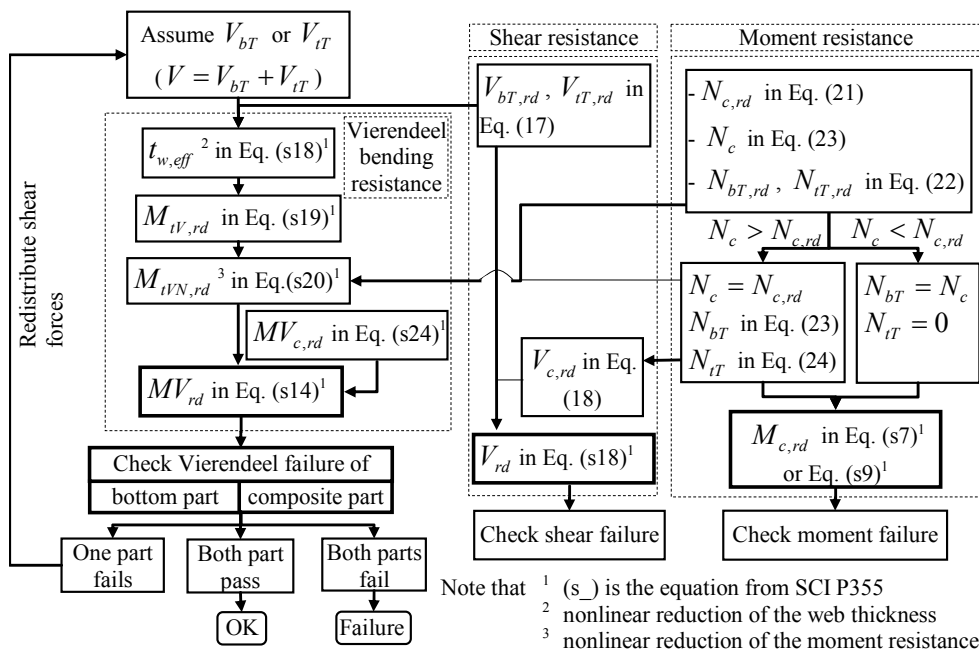


Fig. 3 Force equilibrium in a perforated section

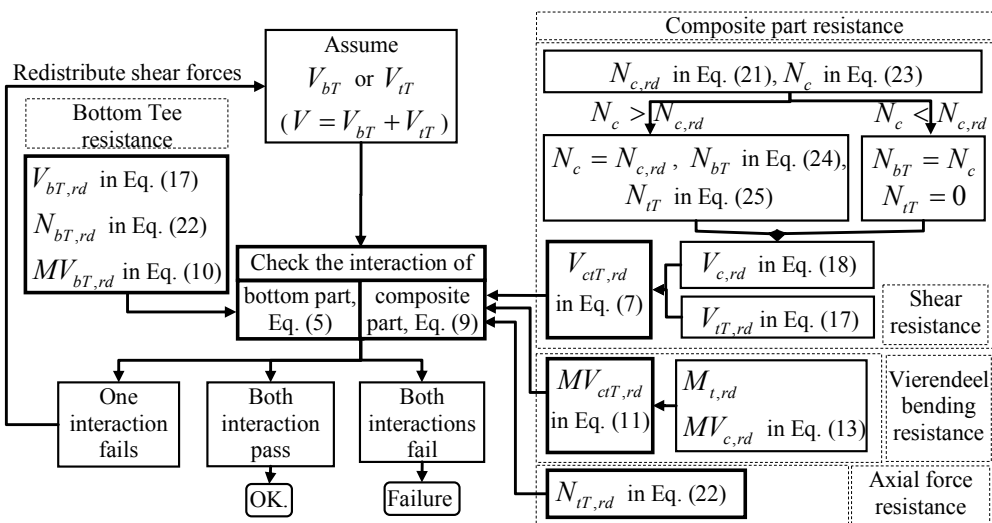
2.4 Axial force and resistance

For a composite beam, the global moment is generally resisted by tension in the bottom Tee and compression in the composite top part. To determine the plastic bending resistance of a perforated composite beam at the opening centerline, the forces in the bottom Tee and the composite top part must be in equilibrium. The tension force in the bottom Tee is firstly balanced by the compression force in the concrete slab. The two cases illustrated in Fig. 3 are possible: the compression resistance of the concrete slab,  $N_{c,Rd}$ , is greater or lesser than the tension force of the bottom Tee,  $N_{bT}$ .

The slab compression resistance (Lawson 2011) is limited to the compression resistance of an effective slab width,  $b_{eff}$ , and the longitudinal shear resistance provided by



(a) Procedure of SCI P355



(b) Procedure of the proposed method

Fig. 4 Procedures to check the Vierendeel failure

Table 1 Details of the experimental beams

Specimen	Steel beam										Slab		Shear stud		Material			Load			
	$h_{iT}$	$h_{bT}$	$b_f$	$t_w$	$t_f$	$l_o$	$h_o$	$l_{so}$	$L$	$h_p$	$h_c$	$b$	$h_{sc}$	$s_{sc}$	$f_{yf}$	$f_{yw}$	$f_c$	$P_{rd}$	$LP$	$V$	
	mm	mm	mm	mm	mm	mm	mm	m	m	mm	mm	mm	mm	mm	Mpa	Mpa	Mpa	kN	m	kN	
PB1	177.9	177.9	171.5	7.3	11.5	406.6	203.2	2.134	7.315	-	101.6	1219	76.2	350	240	240	48.3	101	2.743, 4.752	113	
PB2	226.7	226.7	190.5	8.7	12.3	549.3	274.6	0.914	4.570	-	101.6	1219	76.2	240	315	315	30.8	101	1.829, 2.743	200	
PB3	231.7	231.7	152.4	9.7	15.7	549.3	274.6	1.829	6.401	-	101.6	1219	76.2	270	278	278	32.3	101	2.743, 3.658	180	
PB4	173.5	173.5	169.9	7.5	12.5	406.4	203.2	0.914	4.572	-	101.6	1219	76.2	250	285	285	27.7	101	1.829, 2.743	160	
PB5	262.0	262.0	169.9	7.5	12.5	628.7	314.5	1.067	5.486	76.2	50.8	1219	114.3	304.8	353	353	30.8	60.9	2.896, 3.810	149	
PB6	262.0	262.0	165.3	9.1	11.1	628.7	314.5	1.981	5.486	76.2	50.8	1219	114.3	304.8	342	342	33.4	63.3	2.896, 3.810	158	
PB7	262.0	262.0	165.3	9.1	11.1	628.7	314.5	1.981	5.791	76.2	50.8	1219	114.3	304.8	344	344	32.7	89.5	2.896	153	
PB8	287.5	236.7	165.3	9.1	11.1	628.7	365.5	1.981	5.791	76.2	50.8	1219	114.3	304.8	344	344	35.1	63.3	2.896	113	
PB9	128.7	128.7	101.5	5.9	7.0	300.2	151.1	0.924	3.658	76.2	63.5	1001	127	304.8	320	320	27.2	55.8	1.524	78	
PB10	132.5	124.8	101.5	5.9	7.0	473.2	162.1	0.749	3.658	76.2	63.5	1001	127	304.8	320	320	34.4	48.3	1.524	58	
PB11	262.0	262.0	168.5	9.3	10.8	628.7	374.7	5.181	1.067	76.2	101.6	1219	139.7	304.8	265	265	28.8	47.6	2.591	117	
PB12	265.3	258.7	168.5	9.4	10.9	374.7	374.7	5.181	0.914	76.2	101.6	1219	139.7	304.8	265	265	30.1	49.1	2.591	173	
CB <sub>IT</sub>	305.0	-	190	9.4	14.6		1105	425	15.26	7.63	80	70	3000	125	300	410	410	24.0	64	1.908, 5.732, 8.029, 13.752	126
CB <sub>bT</sub>	-	260.0	300	12.5	22.5																

\* Note: - PB1-4 were tested by Clawson and Darwin (1980), PB5-12 were tested by Donahey and Darwin (1986), and CB were tested by Sheehan *et al.* (2016)

- for specimen CB,  $l_o$  is the full length of the elongated opening, and  $h_o$  is the opening diameter,  $d_o$

the shear studs between the nearest support to the opening centerline, as given in Eq. (21). The axial resistance of the Tees,  $N_{T,rd}$ , is calculated based on the Tee area,  $A_T$ , as given in Eq. (22).

$$N_{c,rd} = \min(0.85f_c b_{eff} h_c, n_{sc} P_{rd}) \quad (21)$$

$$N_{T,rd} = f_y A_T \quad (22)$$

where  $n_{sc}$  is the number of shear studs placed over the distance from a near support to the opening centerline.

In case the compression resistance of the concrete slab is greater than the tension force of the bottom Tee, no tension or compression forces in the top Tee are assumed. The compressive force in the concrete slab,  $N_c$ , and the tension force in the bottom Tee,  $N_{bT}$ , can be simply computed as in Eq. (23).

$$N_{bT} = N_c = \frac{M}{h_{eff} + z_{iT} + h_s - 0.5h_c} \leq N_{bT,rd} \text{ and } N_{c,rd} \quad (23)$$

where  $h_{eff}$  is the distance between centroids of the top and bottom Tees, and  $z_{iT}$  is the distance from centroid of the top Tee to outer face of the flange.

If the compression resistance of the concrete slab is less than the tension force of the bottom Tee, the compression force of the concrete slab reaches its resistance and equilibrium is achieved by developing compression in the top Tee. Uniformly compressive stress in the top Tee can be conservatively assumed. For this case, the tension force of the bottom Tee,  $N_{bT}$ , and the compressive force of the top Tee,  $N_{iT}$ , can be simply computed as in Eqs. (24) and (25).

$$N_{bT} = \frac{M - N_{c,rd}(z_{iT} + h_s - 0.5h_c)}{h_{eff}} \leq N_{bT,rd} \quad (24)$$

$$N_{iT} = N_{bT} - N_{c,rd} \leq N_{iT,rd} \quad (25)$$

The procedures to check the Vierendeel failure of SCI P355 and the proposed method are summarized in Figs. 4(a) and (b). SCI P355 requires the web thickness reduction due to the effects of shear loads, and requires the moment resistance reduction of the Tee due to the effects of axial forces. The moment, shear and Vierendeel bending failures are separately checked. In the proposed method, no nonlinear reductions are required. Combination of bending moment, shear force and Vierendeel bending moment is simultaneously addressed in this method.

### 2.5 Vierendeel bending resistance for circular openings

Procedures to check the Vierendeel failure for a composite beam with a circular opening is same as cases with a rectangular opening as summarized in Fig. 4. However, for circular openings, an equivalent rectangular opening is recommended for simple estimates of the Vierendeel bending moment and its resistance (Lawson 2011). The length of equivalent opening,  $l_o$ , in Eq. (26) and the height of equivalent opening,  $h_o$ , in Eq. (27) are used for a composite beam with circular or elongated web openings, as shown in Fig. 5.

$$\begin{aligned} l_o &= 0.45d_o && \text{for circular openings} \\ l_o &= l_{eo} - 0.55d_o && \text{for elongated openings} \end{aligned} \quad (26)$$

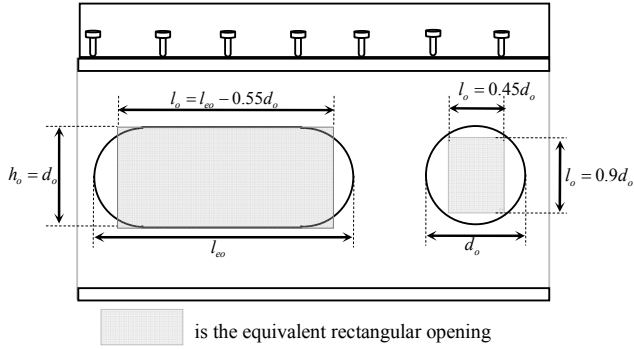


Fig. 5 Equivalent opening of circular or elongated web openings

$$\begin{aligned} h_o &= 0.9d_o && \text{for circular openings} \\ h_o &= d_o && \text{for elongated openings} \end{aligned} \quad (27)$$

where  $d_o$  is the opening diameter,  $l_{eo}$  is the full length of the elongated opening. The equivalent height in Eq. (27) is also used to compute the bending and axial resistances of the sections above and below the opening. However, the shear resistance of a composite or non-composite beam with circular web openings is computed based on the full height of the circular opening.

### 3. Experimental validation

The proposed method was validated against experimental results of 13 composite steel beams with web openings (Clawson and Darwin 1980, Donahey and Darwin 1986, Sheehan *et al.* 2016). Details of the steel beam specimens of Clawson and Darwin (1980), and Donahey and Darwin (1986) were reported in (Ko 2002). There were 12 perforated composite steel beams with rectangular openings and one composite cellular beam with elongated openings. All specimens were composite steel beams with a simple support. As reported in the literature, the Vierendeel failure was found in all the beams.

The experimental parameters are documented in Table 1. Geometric details of the beams are shown in Fig. 6. The specimen labels PB and CB refer to perforated beams with a rectangular opening, and cellular beams with an elongated circular opening, respectively. The subscripts  $tT$  and  $bT$  of specimen CB refer to the section above and below the

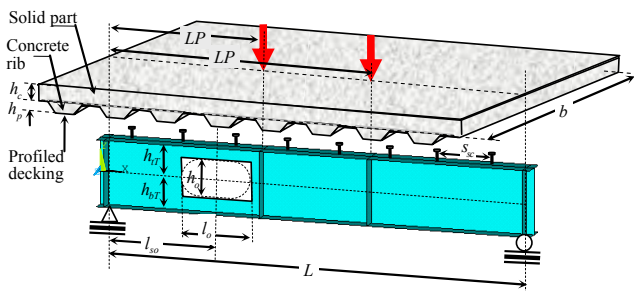


Fig. 6 Geometric details of specimens

opening centerline. The experimental parameters are as follows:  $h_{tT}$  and  $h_{bT}$  are the depths of the steel sections above and below the opening centerline,  $b_f$  is the flange width,  $t_w$  and  $t_f$  are the web and flange thicknesses,  $l_o$  and  $h_o$  are the opening width and height,  $L$  is the beam span length,  $LP$  is the distance between the point load to the left support,  $l_{so}$  is the distance from nearest support to the opening centerline,  $h_{sc}$  and  $s_{sc}$  are the nominal height and spacing of shear studs,  $f_{y,w}$  and  $f_{y,f}$  are the yield stresses of the webs and the flanges, and  $f_c$  is the cylinder compressive strength of concrete. Note that  $h_{tT}$  and  $h_{bT}$  are not equal in specimens which their web opening is not located at mid-height of the web. It is called eccentric opening. To distribute the concentrated load, web stiffeners were welded at the beam supports and the point load location for all specimens, with the exception of specimen CB. Solid concrete slabs were used in specimens PB1-PB4, whereas concrete slabs with profiled sheeting transverse to supporting beams were used in the other specimens. In specimen CB, some web openings were fully or partially closed to avoid local failures on loading. The opening spacing,  $s$ , in specimen CB is 680 mm.

Shank diameter of all shear studs,  $d_{sc}$ , is 19 mm, with the exception of specimens PB9 and PB10 that have 15.9 mm diameter. The ultimate strength of the shear studs,  $P_u$ , is assumed to equal 450 MPa. Most specimens have two shear studs per rib; only the specimens PB7, PB9 and CB have one shear stud per rib. Since the experimental shear resistance of the stud was not reported in the literature, the nominal unfactored design shear resistance of the stud,  $P_{rd}$ , based on EN 1994-1-1, given in Eq. (28), is used here instead. For slabs with profiled sheeting transverse to supporting beams, a reduction factor,  $k_t$ , is required as in Eq. (29). The design rules for  $P_{rd}$  based on EN 1994-1-1 are generally less conservative comparing with experimental results or numerical simulations in the literature (Ellobody and Young 2006).

$$P_{rd} = k_t 0.29 \alpha d_{sc}^2 \sqrt{f_c E_c} \leq 0.8 f_u (\pi d_{sc}^2 / 4) \quad (28)$$

$$k_t = \frac{0.7}{\sqrt{n_r}} \left( \frac{b_o}{h_p} \right) \left( \frac{h_{sc}}{h_p} - 1 \right) \quad (29)$$

where  $\alpha$  is the reduction factor on the shear resistance due to  $h_{sc} / d_{sc}$  ratio,  $E_c$  is the secant elasticity modulus of concrete,  $n_r$  is the number of the shear studs per rib in the transverse decking, and  $b_o$  is the average trough width of decking rib. Note that  $\alpha = (h_{sc} / d_{sc} - 1)$  and  $\alpha = 1$  for  $3 \leq h_{sc} / d_{sc} \leq 4$  and  $h_{sc} / d_{sc} > 4$ , respectively.

The Vierendeel failure of a composite beam depends on the shear force transfer and the pull-out acting in the slab, which is compatible with the relative deflection across the opening,  $\Delta$ . The criterion  $\Delta = l_o / 60$  was specified to determine the Vierendeel failure in Lawson *et al.* (2013). This study also applies the same criterion to identify the Vierendeel failure of the specimens, and later on comparing with finite element analysis. Note that, based on the finite element investigation on the Vierendeel failure in the next section, yielding of the sections surrounding the opening is

Table 2 Shear load results

Specimen	$h_o/H$	$l_o/h_o$	Failure shear loads (kN)				$V/V_{Test}$			
			Test	PPM	SCI P355	FE	PPM	SCI P355	FE	
PB1	0.57	2.00	112.7	102.9	70.1	104.0	0.91	0.62	0.92	
PB2	0.61	2.00	199.9	150.5	126.0	198.4	0.75	0.63	0.99	
PB3	0.59	2.00	179.9	144.7	119.9	189.9	0.80	0.67	1.06	
PB4	0.59	2.00	159.7	115.8	94.8	167.1	0.72	0.59	1.05	
PB5	0.60	2.00	149.2	139.7	132.3	147.0	0.94	0.89	0.99	
PB6	0.60	2.00	158.0	148.7	136.3	146.3	0.94	0.86	0.93	
PB7	0.60	2.00	152.9	140.4	126.5	144.9	0.92	0.83	0.95	
PB8	0.70	1.72	112.9	116.2	105.3	121.4	1.03	0.93	1.08	
PB9	0.59	1.99	78.2	61.1	49.5	76.8	0.78	0.63	0.98	
PB10	0.63	2.92	58.2	55.4	44.0	64.3	0.95	0.76	1.10	
PB11	0.72	1.68	117.1	110.0	78.2	127.4	0.94	0.67	1.09	
PB12	0.72	1.00	172.8	143.3	107.3	181.5	0.83	0.62	1.05	
CB	0.75	2.60	136.9	118.2	96.1	136.7	0.86	0.70	1.00	
							Mean	0.88	0.72	1.01
							STD	0.09	0.12	0.06
							COV	0.10	0.16	0.06

also observed at this relative deflection. Therefore, this criterion appears appropriate to identifying initiation of the failure. In Table 1, the experimental failure shear load at the opening centerline,  $V$ , is the sum of the experimental shear load at  $\Delta = l_o / 60$  and the shear load from the specimen self-weight.

The experimental failure shear load was used to validate the accuracy of Vierendeel bending resistance predictions by the proposed method. The shear loads computed from SCI P355 were also investigated to compare the accuracy. Their statistics such as mean, standard deviation (SD) and coefficient of variation (CV) are shown in Table 2. The opening depth ratios,  $h_o/H$ , and the opening width ratios,  $l_o/h_o$ , are also reported in the table, where  $H$  is the steel beam depth. Since the root radius of rolled steel section is not reported in the literature for most of the specimens, the shear resistances were conservatively estimated without the root radius parameter.

As seen in the table, the failure shear loads of the proposed method (PPM) are close to the experimental results and significantly less conservative than estimates from SCI P355. On an average, the shear loads of the proposed method and SCI P355 are conservative by about 12% and 28%, respectively. Compared to the proposed method, SCI P355 provides slightly lower shear loads for opening depth ratios  $h_o/H$  of about 0.6, and for opening width ratios  $l_o/h_o$  of about 2, but tends to provide very conservative results for other ratios.

The experimental results curated from literature are limited in scope. To examine the limitations and the accuracy of the proposed method for predicting the resistance, effects on the failure shear load of beam parameters outside the range covered by prior literature should be further investigated. For this reason, a parametric study was performed by using finite element simulations.

#### 4. FE investigation

Effects on Vierendeel failure of the stud properties, the geometric configuration of the steel beams, the web openings, and the concrete slab were investigated through finite element (FE) simulations. The FE models were validated against the experiments in Table 1. The criterion  $\Delta = l_o / 60$  was also used to determine the Vierendeel failure initiation in the FE simulations.

##### 4.1 FE modeling and validation

A non-linear finite element model was set up using ANSYS software. Steel beams were modeled using Shell181 elements (ANSYS 2007). Since the study focuses on global behaviors of the Vierendeel failure rather than local failures in the concrete slab, such as concrete cracking or crushing, the concrete slab was also modeled using Shell181 elements. Shell181 element is a four-node shell element having six degrees of freedom at each node—nodal rotations and translations in the  $x$ ,  $y$ , and  $z$ - axes. This shell element is appropriate for analyzing thin shell structures with linear or nonlinear characteristics.

Due to weakening of the concrete ribs in profiled decking, shown in Fig. 6, only the slab thickness of the solid part was conservatively simulated as a concrete shell layer. The layer was offset to the mid-height of the solid slab above the steel beam, as shown in Fig. 7. Such offset shell layers have been used on simulating composite beams (Bake 2010, Lawson *et al.* 2013).

In order to simulate composite actions of the concrete slab and the steel beam, the shear studs at the steel/concrete interface were simulated as spring elements, with Combine39 elements, for shear and axial deformation. This element is a uniaxial element defined by two nodes with

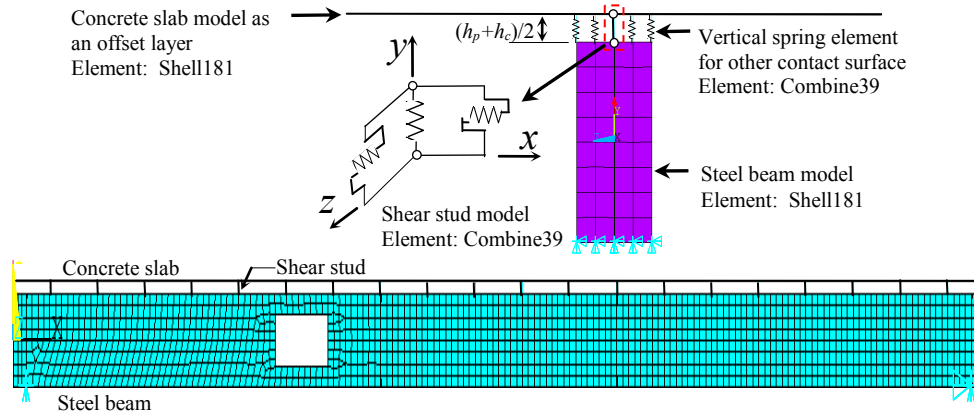


Fig. 7 FE model of a composite beam

nonlinear generalized force-slippage capability accounting for large displacements (ANSYS 2007). As shown in Fig. 7, there are three spring elements used to simulate the force resistance of one stud. The two horizontal spring elements were specified to resist the shear force in parallel (longitudinal) and perpendicular directions, whereas the vertical spring element was specified to resist the pull-out force. The pull-out resistance  $P_{v,rd}$  was taken as half of the shear resistance,  $P_{rd} / 2$  (Lawson *et al.* 2013, Wang and Chung 2008). Furthermore, for other steel/concrete contact surfaces, special Combine39 elements were used to transfer the compression forces from the concrete slab to the steel beam, but without pull-out or tension forces. Movement towards the beam is prevented in this model.

As given in BS EN 1992-1-1, the concrete stress–strain curve was specified as a parabolic rectangular curve. For the steel, the initial linear elastic modulus,  $E_s$ , was taken as 200 GPa with a reduction to 2 GPa ( $0.01E_s$ ) at yield point. The ultimate stress was here set to 1.2 fold yield strength (Panedpojaman *et al.* 2014). The Poisson's ratio was fixed at 0.2 and 0.3 for concrete and steel, respectively.

Since no experimental shear load–slippage curves of the shear studs is available in the literature, the analytical load–slippage curve based on Eq. (30) (Gattesco 1999) was used in the FE model.

$$F_s = P_{rd} \left(1 - e^{-\beta s}\right)^\alpha \quad (30)$$

where  $F_s$  is the shear force in the shear stud at a given slippage  $s$  (mm);  $\alpha$  is a non-dimensional parameter between 0.5 and 1.5, and  $\beta$  is a parameter ( $\text{mm}^{-1}$ ) between 0.5 and 2.0. Due to a wide range of the parameter  $\alpha$  and  $\beta$ , an approximated  $\alpha$  of 1.2 and  $\beta$  in Eq. (31) were used in this study based on the average from 10 experimental load–slippage curves from push-out tests in the literature (Ellobody and Young 2006, Mirza and Uy 2010, Nguyen and Kim 2009, Lawson *et al.* 2013, Lin *et al.* 2014), as shown in Fig. 8. The pull-out load–slippage curve was derived by substituting  $P_{rd}$  with  $P_{v,rd}$  in Eq. (30).

$$\beta = -0.38 \ln(s) + 1.4 \quad (31)$$

Due to fabrication and cutting of steel beams, geometric

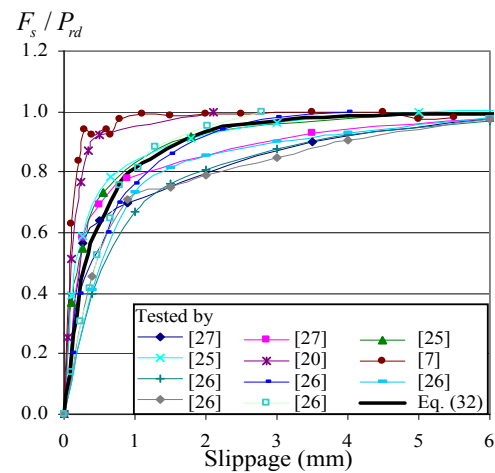


Fig. 8 Experimental load-slippage curve

imperfections affect the load bearing capacity of steel beams. Based on the first mode of elastic eigenvalue analysis, an imperfection pattern was set in the simulation. Therefore, an eigenvalue analysis was firstly conducted before the inelastic analysis. The imperfection amplitude  $H/500$  (Panedpojaman *et al.* 2014) of the first mode was imposed on the initial geometry in this study. The inelastic analysis was conducted by using the Newton–Raphson iterative method. To define the yield point of steel, the Von Mises yield criterion was used.

Before their use in further investigations, the FE models were validated against the experiments in terms of the failure mode, the failure shear load, and the load–deflection curves at the points reported in the literature. Since the opening perforation causes asymmetry in the geometry (left–right) in the specimens, the FE models with the full beam length were simulated.

All the FE models of the experimental cases had Vierendeel failure mechanism, reproducing the experiments in this qualitative sense. Since the analytical results of the beams are similar, the failure modes and the Von Mises stress distributions of specimens PB4 and CB are shown in Fig. 9 as examples. At the failure criterion  $\Delta = l_o / 60$ , formation of plastic hinges was observed in both the top composite part and the bottom steel part, matching the

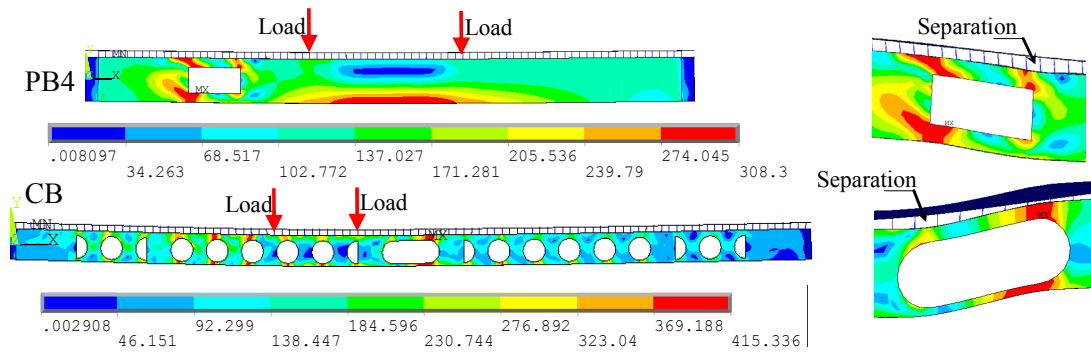


Fig. 9 Failure behavior and Von Mises stress distribution in specimens PB4 and CB

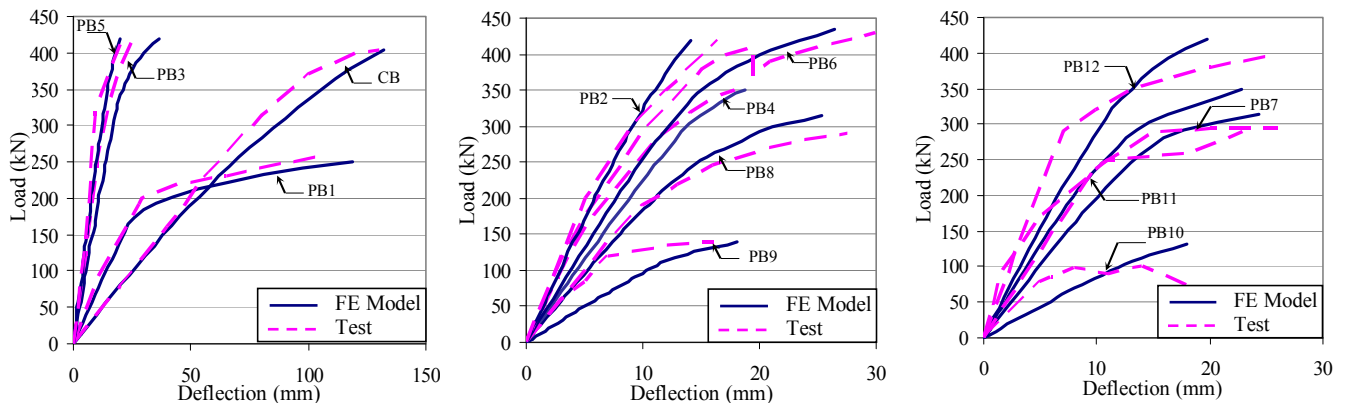


Fig. 10 Shear load vs. deflection curves

Vierendeel mechanism. A large yielding area occurred in the low moment side. Due to relative stiffnesses of the concrete slab and the beam at the opening, also separation was observed as in the pull-out mechanism.

The FE shear loads at the criterion are shown in Table 2, whereas the FE load vs. deflection curve at a given point is illustrated in Fig. 10. The given points are at the mid-span for specimens PB1-PB4 and CB and at the point load near mid-span for specimens PB5- PB12. On an average, the failure shear loads from FE analysis,  $V_{FE}$ , agree well with the experimental results,  $V_{Test}$ . In Table 2, the average  $V_{FE} / V_{Test}$  is 1.01 with standard deviation 0.06. The analytical load–deflection curves are slightly softer than the experimentally observed ones. The main reason may be due to simulating of the slab as a layer and neglecting the concrete ribs. However, overall the FE load–deflection curves agree well with the experiments. Note that deviations of the FE results from the experimental results may be also due to limitations of the experimental data, such as imperfections and material properties.

#### 4.2 Parametric study

A parametric simulation study by using the validated FE models was conducted to investigate effects of beam parameters on the Vierendeel behavior as well as limitations and accuracy of the proposed method for predicting the Vierendeel bending resistance. The parametric study focused on effects of the beam geometry, the opening geometry and the steel properties on the resistance. The steel

grade S355 with  $f_y = 355$  MPa, the concrete cylinder compressive strength of 33 MPa, 70-mm depth of the deck profile, the shear studs with the ultimate strength of 450 MPa and the shank diameter of 19 mm were mainly employed throughout this parametric study. The concrete slab width was specified as 10 times the flange width,  $10b_f$ . The material models in the parametric study were as described in the previous section. The composite beams in this study were simply supported and had a point load at mid-span. All FE models were simulated with the full beam length. A total of 236 composite beam models with web openings were simulated. The parameters varied in the simulations were as follows:

- steel beam sections of the perforated beams and the asymmetric cellular beam;
- concrete slab thickness;
- opening depth ratios  $h_o/H$  or  $d_o/H$ ;
- opening length ratio  $l_o/h_o$ ;
- eccentric level from the mid-height of the beam;
- opening shape, i.e., rectangular, circular or elongated circular opening;
- force-slippage curve of the shear stud; and
- beam length and opening locations to generate at least four different levels of shear and moment utilization at the opening.

Varying the beam length and the opening location is also necessary to ensure that the failure occurs at the opening. If the beam is too long or the opening location is too close to

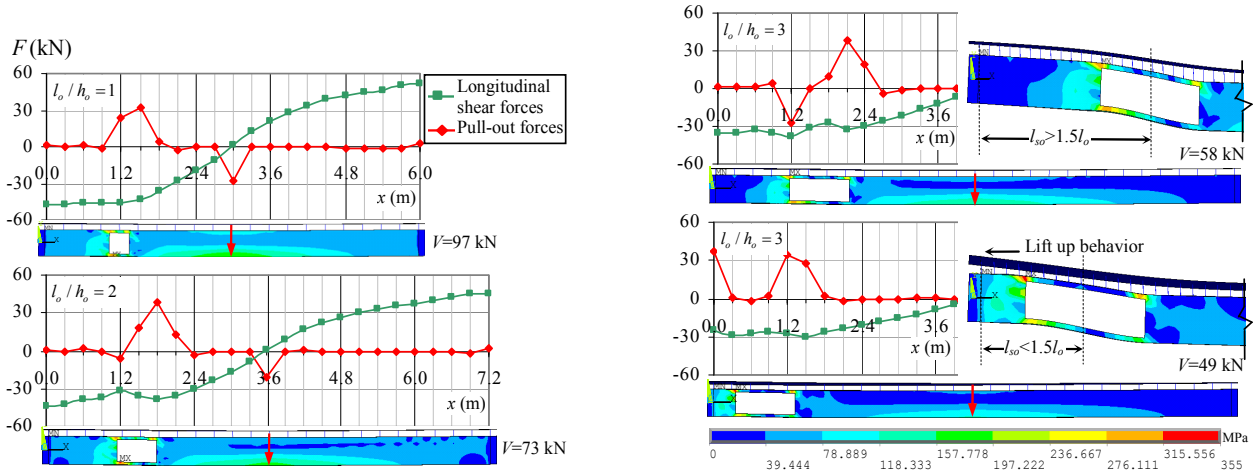


Fig. 11 Distributions of the longitudinal shear force and the pull-out force

the mid span, the beam may fail by moment failure.

#### 4.2.1 Beam and opening geometry

For the perforation cases, the section IPE400 and HEB 400 were simulated. The section ratios,  $A_{t,w} / A_{t,f}$  of IPE400 and HEB 400 are 0.71 and 0.38, respectively. Both sections have the same height. The large section ratio illustrates that the web area is large compared to the flange area. The web area,  $A_{t,w}$ , and the flange area,  $A_{t,f}$ , mainly represent the shear and moment resistance, respectively. The section ratio was found to affect some structural behavior of steel beams (Panedpojaman and Thepchatri 2013, Panedpojaman *et al.* 2016). The ratios cover normal uses of hot-rolled steel sections. The models had a rectangular web opening with the opening depth ratios  $h_o / H$  of 0.5, 0.65 and 0.8, and the opening length ratios  $l_o / h_o$  of 1, 2 and 3. The openings were located at the mid-height of the steel beam for all models. A solid slab with 70-mm depth and stud spacing of 300 mm was used. A total of 72 perforated composite beams were simulated in this investigation. The beam length was in the range from 1.8 to 9.6 m.

Distributions of the longitudinal shear force, the pull-out force, and the Vierendeel behavior were investigated first. Due to similarity of these simulation results, only the distributions of the IPE400 model with  $h_o / H$  of 0.8 and  $l_o / h_o$  of 1, 2 and 3 are illustrated in Fig. 11. It can be observed that the longitudinal shear force increases with distance from the mid span and undulates around the opening. The longitudinal shear force reaches its maximum at the beam end. The maximum of the longitudinal shear forces along the opening length takes place at about mid-opening and the force decreases towards either edge of the opening. At the failure criterion  $\Delta = l_o / 60$ , the maximum shear force of the stud in all FE models was about 60% of the stud shear resistance  $P_{rd}$ , and there was no longitudinal shear failure in the simulations. The stud pull-out forces are concentrated around the opening edge of the higher moment side. The maximum pull-out force depends on the stud location and the opening geometry. The average maximum pull-out force in all FE models was consistently about 75% of the pull-out resistance  $P_{v,rd}$ . Based on the force utilization, the pull-out failure should be more concerned

than the longitudinal shear failure.

For the models with distance from the nearest support to the opening centerline,  $l_{so}$ , less than 1.5 times the opening length,  $l_{so} < 1.5l_o$ , the FE failure loads were significantly below the cases with inner opening. As shown in Fig. 11, the maximum pull-out force takes place at the slab end whereas the longitudinal shear force still behaves similarly to the other cases. Lift-up of the concrete slab at the support was observed. This indicates that the pull-out forces over the distance are not sufficient to restrain the concrete slab in place. Concrete crushing is incomplete at initiation of Vierendeel failure, so the Vierendeel bending resistance contribution by concrete crushing in Eq. (21) must be neglected when  $l_{so} < 1.5l_o$ .

The estimates of Vierendeel bending resistance in terms of failure shear loads from the FE model ( $V_{FE}$ ) and from the proposed method ( $V_{PPM}$ ) are compared in Fig. 12. The proposed method provides generally conservative resistance estimates. The failure loads are high in cases of short or/and narrow opening whereas the failure loads are low in cases with tall or/and wide openings. Since the moment arm is

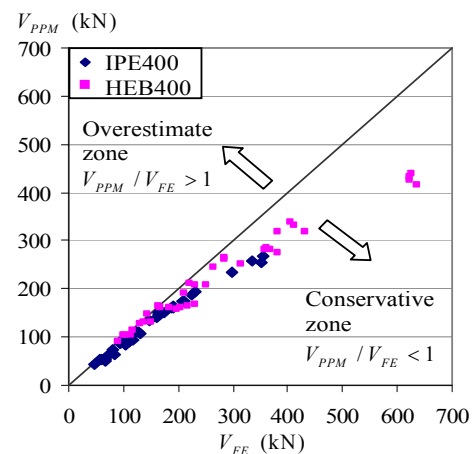


Fig. 12 Comparison of the FE failure shear load estimates with the resistance estimates from analytical formulas, across various beam and opening geometries

small with a narrow opening, the Vierendeel bending moment is low and affects the beam failure comparatively little: as a result, the failure shear loads are high. On the other hand, the Vierendeel bending resistances are high with short openings due to the deep Tee sections above and below the opening. Therefore, the short opening cases can resist higher loads than those with tall opening. The same explanation applies to the low failure loads of the cases with tall or/and wide opening.

Variation of the shear load utilization,  $V_{PPM} / V_{rd}$ , with the shear load ratio of  $V_{PPM}$  to  $V_{FE}$  is shown in Fig. 13(a). It can be observed that, at high load utilization with  $V_{PPM} / V_{rd} > 0.7$ , the proposed method provides significantly conservative results,  $V_{PPM} / V_{FE} \ll 1$ . In cases with high failure shear load, i.e., high shear load utilization, the shear force mainly affects the failure, not Vierendeel bending. The computed shear loads of sections IPE400 and HEB400 are conservative by up to 27% and 35%, respectively, relative to the FE failure loads. The severely conservative level of the computed shear loads may be due to the conservative shear resistance from BS EN 1993-1-1, reported in Panedpojaman *et al.* (2015). When Vierendeel bending dominantly affects the failure (the failure shear load is low, that is low shear load utilization), the prediction accuracy improves. The  $V_{PPM} / V_{FE}$  ratios are in the range from 0.76 to 0.97 for section IPE 400, and from 0.72 to 1.03 for section HEB 400. The section ratio slightly affects accuracy of resistance estimates. The proposed method provides conservative estimates for both sections, on average by about 15%.

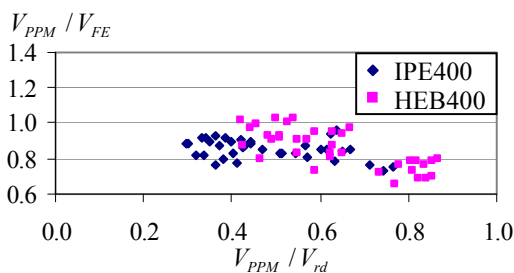
In the rigid-plastic model (Lawson *et al.* 2013), an effective slab width  $b_{eff}$  was recommended for computing the Vierendeel bending resistance. The resistance obtained from the proposed method with  $b_{eff}$  (PPM- $b_{eff}$ ) is also

compared in Fig. 13(b). Generally, the PPM- $b_{eff}$  method gives less accurate resistance predictions, especially in cases with low load utilization. Also severe overestimates of the resistance can be observed in the figure. Therefore, it is suggested that  $b_{eff}$  should not be used in the computations.

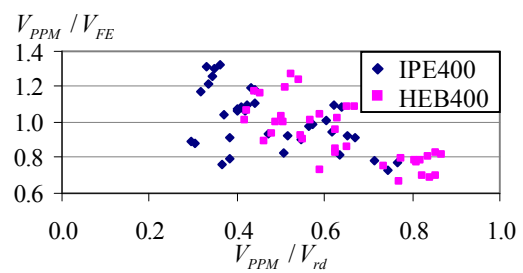
#### 4.2.2 Eccentric opening

To investigate effects of eccentric opening in the web, the openings of all IPE 400 models were moved up or moved down by 10% or by 5% of the beam height, for the cases with  $h_o / H$  of 0.5 and 0.65, or 0.8, respectively. The FE failure shear loads with moved-up opening (positively eccentric),  $V_{FE,e+}$ , and with the moved-down opening (negatively eccentric),  $V_{FE,e-}$ , are compared with the FE failure shear loads with neutral opening,  $V_{FE}$ , in Fig. 14(a). It can be observed that the failure loads in the eccentric cases, especially in the moved-up cases, are generally higher than in the neutral cases.

Two mechanisms of the eccentric opening can be elaborated. Firstly, an eccentric opening causes greater Vierendeel bending resistance in the deeper Tee section and lesser resistance in the other Tee. However, the sum of the resistances based on Eq. (11) is higher than with neutral opening. Therefore, the eccentric cases generally provide higher failure loads than the neutral cases. The other mechanistic effect is that the moved-up opening gives deeper bottom Tee with larger Tee area, which can resist higher tension forces from the global moment. Higher compression forces in the concrete slab are required to balance that tension. Based on Eq. (18), the higher compression forces provide higher shear resistance of the concrete slab,  $V_{c,rd}$ . As a result, the failure loads of the moved-up cases are generally higher than those of the moved-down cases as shown in Fig. 14(a).

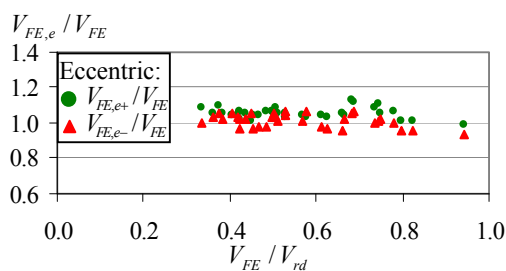


(a) Proposed method

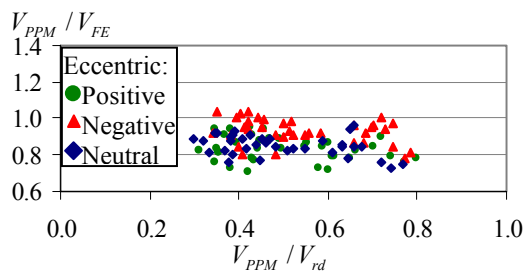


(b) Proposed method with effective slab width  $b_{eff}$ , PPM- $b_{eff}$

Fig. 13 Relation of shear load ratio to shear load utilization, across various beam and opening geometries



(a) FE shear load ratio of eccentric cases to the neutral cases



(b) shear load ratio of the proposed method to the FE model

Fig. 14 Relation of shear load ratio to shear load utilization across various eccentricities

The failure load estimates are shown in Fig. 14(b) with shear load utilization. Overall, the computed resistances conservatively agree well with the FE results. However, the computed resistances in the positively eccentric cases tend to be more conservative than in the neutral cases and the negatively eccentric cases.

#### 4.2.3 Spacing and load–slippage curves of the shear studs

The Vierendeel bending resistances of IPE 400 models with  $h_o/H$  of 0.5, 0.65, and 0.8 and  $l_o/h_o$  fixed at 2 were investigated by varying the spacing and the load–slippage curve of the shear stud. The stud spacings 150 mm and 300 mm were used in the investigation. The load–slippage curve based on Eqs. (30) and (31) as a standard curve was compared with softer and stiffer curves shown in Fig. 15. The slippage of the soft curve is five times that of the standard curve at a given shear force, whereas the shear force of the stiff curve is 1.5 times that of the standard curve at a given slippage. The FE failure load with alternate stud behavior  $V'_{FE}$  to the standard case  $V_{FE}$ , is shown in Fig. 16(a) against the FE shear load utilization. Compared with the standard cases, short spacing and higher shear resistance can improve the FE failure load up to 5% and 15%, respectively. The soft curve of the shear stud degrades the FE failure loads. However, the curve does not affect the computed resistance because only the shear stud resistance, not its curve, is applied in the estimate. As long as the curve

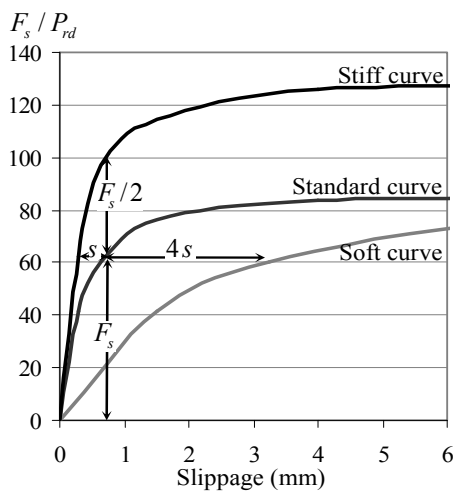
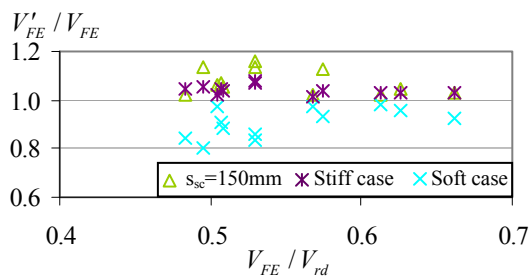


Fig. 15 Load–slippage curves of the shear stud



(a) FE shear load ratio of alternative cases to the standard cases

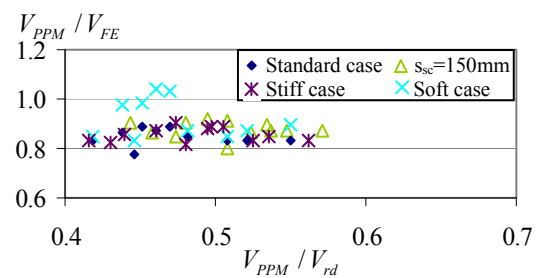
has the same shear stud resistance, the computed resistance does not change. However, when the severely soft curve is used in FE simulation, the failure load is lower than in the standard case by 2–20% and by about 10% on average. It can be concluded that the slippage curve does not dramatically affect the resistance.

The failure load ratio, of the computed resistance to the FE failure load, is shown in Fig. 16(b) against shear load utilization. Generally, the computed resistance is conservative. However, the soft curve clearly degrades the computed resistance from the standard case. In a few cases the computed resistance is slightly higher, by up to 4%, than the FE failure load. Note that on average, the pull-out force at the failure criterion of the standard cases, of the short spacing cases, of the cases with the stiffer curve, and of the cases with the softer curve is 76%, 75%, 71% and 32% of the corresponding pull-out resistance, respectively. The slippage corresponding to the pull-out force at the failure criterion is 0.80, 0.77, 0.67, and 0.75 mm, in the same order. Therefore, at the failure criterion  $\Delta = l_o / 60$ , the shear stud is not subject to completely pull-out failure.

#### 4.2.4 Slab thickness and circular opening

Slab thicknesses 70 and 100 mm of the solid part were used in the investigation. The Vierendeel bending resistances of IPE 400 models with  $h_o/H$  of 0.5, 0.65, and 0.8 and  $l_o/h_o$  fixed at 2 were investigated. The thicker slab provides higher Vierendeel shear resistance in both the FE and computed estimates. Variation of the shear load ratio with the shear load utilization is shown in Fig. 17. It is found that the computed resistance of the thick slab is more conservative than that of the thin slab by about 7% on average. The reason may be that the proposed method underestimates the Vierendeel resistance of concrete slab and its composite action. However, the method can still be used as a conservative prediction.

To investigate the appropriateness of the proposed method for a composite beam with circular opening, the IPE 400 models with  $h_o/H$  or  $d_o/H$  of 0.5, 0.65, and 0.8 were simulated and compared to those with square opening,  $l_o/h_o = 1$ . The concept of an equivalent rectangular opening was applied in the computations. The results are also illustrated in Fig 17. It can be observed that the proposed method again provides conservative estimates. Since the effective opening length is short, especially in models with  $d_o/H$  0.5 and 0.65, Vierendeel bending affects the failure less. The computed resistance is highly conservative due to the



(b) Shear load ratio of the proposed estimate to the FE model

Fig. 16 Relation of shear load ratio to shear load utilization, across various stud properties

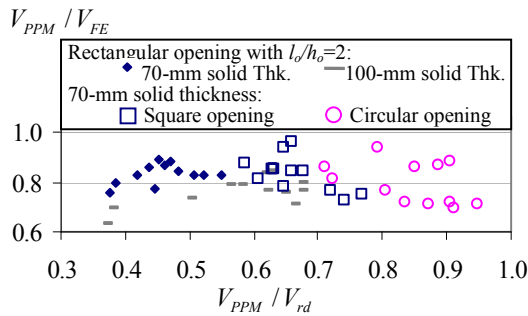


Fig. 17 Relation of shear load ratio to shear load utilization, across various thickness and circular opening parameters

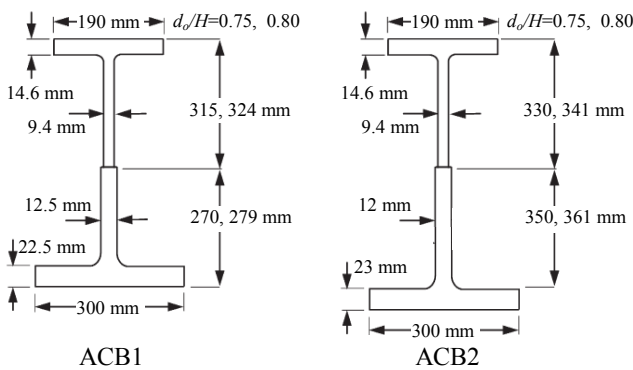


Fig. 18 Geometry of the asymmetric cellular beam

conservative shear resistance used in the computation, as mentioned before. With a large opening, the Vierendeel bending affects the failure more and the computed results are less conservative.

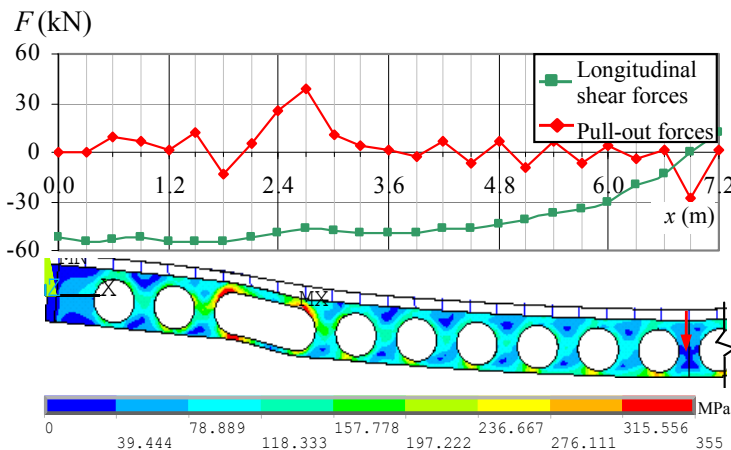
4.2.5 Asymmetric cellular beam

Asymmetric cellular beams ACB1 and ACB2 were simulated as shown in Fig. 18. The sections of beam ACB1 are based on the experiments in (Sheehan *et al.* 2016). Depths of the steel deck profile and the solid slab part for beams ACB1 and ACB2 are the same as for specimen CB in

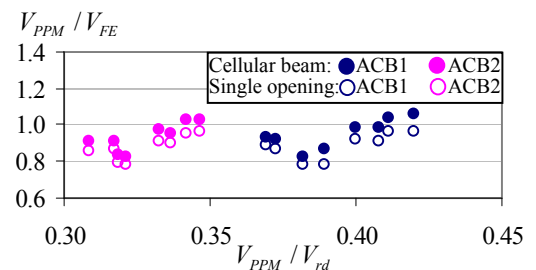
Table 1. However, the other properties are the same as in other cases of the parametric study. The top Tee section of both beams was cut from IPE 450 whereas the bottom Tee section was cut from HEB360 for beam ACB1 and HEA500 for beam ACB2. Sections HEB360 and HEA500 are similar in their web and flange thicknesses. In practice, the top Tee section can be taller or shorter than the bottom Tee section. In this investigation, the beams ACB1 and ACB2 represent cases with taller and shorter top Tee section than the bottom Tee section, respectively. As long span composite cellular beams, they were simulated with length-to-depth ratios in range from 23 to 26. Both beams have a bottom flange area to top flange area ratio about 2.4, which is highly asymmetric. Each beam was modeled with the opening depth ratios  $d_o / H$  of 0.75 and 0.80, as is common in asymmetric cellular beams. An elongated opening comprised of two adjacent openings was used to investigate the Vierendeel failure. The elongated opening location was also varied along the beam length to generate at least four different levels of shear and moment utilization at the opening. A total of 16 asymmetric cellular beams were used in the investigation.

At the failure criterion, distributions of the longitudinal shear and pull-out forces of the stud in ACB1 with  $h_o / H$  of 0.8 are illustrated in Fig. 19(a), as a representative case. The distributions are slightly different from the perforated case shown in Fig. 11. Since weakness of the opening section causes a relative displacement at edges of the openings, the longitudinal shear forces and the pull-out forces undulate. High pull-out forces are concentrated over the elongated opening. The maximum pull-out forces are at the elongated opening on the high moment sides.

The shear load ratio versus shear load utilization is illustrated in Fig. 19(b). The computed resistances are mostly conservative by about 6% on average. There are a few cases such that the proposed method overestimates the resistance by up to 5%. The proposed method provides similarly conservative estimates for both cases, the beams ACB1 and ACB2. Therefore, the method can generally be used for both taller and shorter top Tee section than the bottom Tee section. Note that the estimate for the regular perforated beam in Section 4.2.1 is conservative by about



(a) Distributions of the longitudinal shear forces and the pull-out forces



(b) Relation of shear load ratio to shear load utilization

Fig. 19 Numerical results for the asymmetric cellular beam

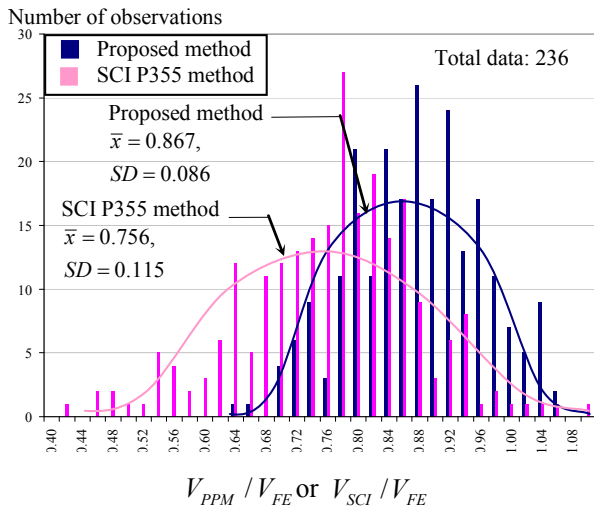


Fig. 20 Normal distribution of the normalized design resistance for each method

15%. The less conservative estimates may be due to interactions of the Vierendeel bending mechanism in the perforated sections and the web-post buckling mechanism in the web-post between adjacent openings (Panedpojaman *et al.* 2014). To confirm such effect, further 16 models were simulated with single elongated openings, without other openings. It was found that the computed resistances for single elongated openings are conservative by about 12% on average, which is close to the cases in Section 4.2.1.

#### 4.2.6 Proposed method and SCI P355

In summary, there were 204 models of perforated beams and 32 models of asymmetric cellular beams assessed. Distributions of the normalized design resistance from the proposed method ( $V_{PPM}$ ) and from SCI P355 ( $V_{SCI}$ ) with the FE failure load ( $V_{FE}$ ) are shown in Fig. 20.  $V_{PPM} / V_{FE} = 1$  or  $V_{SCI} / V_{FE} = 1$  indicates the estimate equal to that from FE simulation. Based on averages and standard deviations, the fitted normal distributions are also plotted. The averages for the proposed method and SCI P355 are 0.867 and 0.756, respectively. The proposed method is significantly less conservative. The wide spread of SCI P355 indicates that its predictions are inaccurate. In contrast, the proposed method conservatively provided the narrow spread with small standard deviation. It means the predictions of the proposed method are more accurate and consistently safe. Note that the proposed method slightly overestimates the resistance by up to 5% in some cases, especially for asymmetric cellular beams. SCI P355 provides significantly conservative results by up to 58% for deep and long opening cases, whereas the proposed method provides significantly conservative results by up to 36% for short and narrow opening cases.

## 5. Conclusions

To develop a simple and effective design method for the Vierendeel bending resistance of composite beams with

web openings, an alternative design method was proposed. The proposed method was mainly derived by using quadratic nonlinear interaction of normalized three co-existing actions that contribute to the resistance. The actions relate to shear force, axial force and Vierendeel bending moment.

The composite beams were separated into the top Tee section and the bottom Tee section. The interactions of these sections must be considered to prevent the Vierendeel failure. This study assumed that the shear load and the Vierendeel bending moment are distributed based on its resistances. Therefore, the normalized shear force and Vierendeel bending moment of the top tee section and the composite part are the same. The normalized force and moment of the composite part can be used in the interaction instead. The normalized axial force was computed based on force equilibrium. The axial force due to the global moment is mainly resisted by the concrete slab and later resisted by the steel top Tee section. By using the proposed method, nonlinear reductions of web thickness (due to effects of the shear loads) and nonlinear reductions of the moment resistance of the Tee (due to effects of the axial forces) are not required as in prior methods. The combined bending moment, shear, and Vierendeel bending moment is simultaneously addressed in the novel method.

The resistances to the axial and shear forces were directly computed based on a standard. The Vierendeel bending resistance for the composite beams is a combined bending resistance of the Tee sections above and below the opening at the four opening corners, and the composite resistance. The bending resistance at the vertical centerline of an opening corner was used to compute the bending resistance of the Tee. Based on a rigid-plastic model which considers the pull-out of shear studs and crushing in the concrete slab, the composite resistance was computed. This study proposed that an appropriate slab width for computing the composite resistance is the effective slab width of the vertical shear resistance, not of the compressive resistance.

The accuracy of the proposed method was validated against 13 experiments curated from literature in terms of the shear load at the failure. As recommended in the literature, the initiation of failure was assumed at 1/60 relative displacement between the opening edges. To investigate the limitations and accuracy of the proposed method, 236 finite element (FE) composite beam simulations were run. The varied beam sections included composite asymmetric cellular beams, alternative opening shapes and locations, eccentric openings, different concrete slab thicknesses and shear stud properties. The design loads from SCI P355 and from the proposed method were compared to the FE simulations. On average, the design load from SCI P355 and from the proposed method was 0.756 and 0.867 times the FE failure load, respectively. Compared to SCI P355, the proposed method is significantly less conservative with smaller estimation errors. The predictions by the proposed method are comparatively accurate. Generally, the investigated parameters did not much affect the prediction accuracy of the proposed method. Severely conservative critical load estimates by up to 36% were found in cases with short and

narrow openings. Slightly overestimated loads by up to 5% were found in cases with tall and wide openings, and with asymmetric cellular beams.

The proposed method allows practical and simple design computations of Vierendeel failure limits for a composite beam with web openings. Compared to prior methods, the proposed method improves the prediction accuracy of Vierendeel bending resistance and enables more economical designs.

## Acknowledgments

The authors sincerely thank Assoc. Prof. Dr. Seppo Karrila and the copy-editing service of the Research and Development Office, the Prince of Songkla University for their support and valuable comments.

## References

- ANSYS (2007), ANSYS Guide - Release 11.0 Documentation, Ansys Inc.
- Bake, S. (2010), "Cellular beams at ambient and elevated temperatures", Ph.D. Dissertations; School of Mechanical, Aerospace and Civil Engineering, MACE, The University of Manchester, Manchester, UK.
- BS EN 1993-1-1 (2005), Eurocode 3: Design of Steel Structures Part 1-1: General Rules and Rules for Buildings, British Standards Institution.
- BS EN 1992-1-1 (2004), Eurocode 2: Design of Concrete Structures - Part 1-1 : General Rules and Rules for Buildings, British Standards Institution.
- BS EN 1994-1-1 (2004), Eurocode 4: Design of Steel and Concrete Composite Structures. Part 1.1: General Rules and Rules for Building, British Standards Institution.
- Clawson, W.C. and Darwin, D. (1980), "Composite Beams with Web Openings", SM Report No 4; University of Kansas Centre for Research, USA.
- Chung, K.F. and Lawson, R.M. (2001), "Simplified design of composite beams with large web openings to Eurocode 4", *J. Constr. Steel Res.*, **57**(2), 135-163.
- Chung, K.F., Ko, C.H. and Wang, A.J. (2005), "Design of steel and composite beams with web openings—verification using finite element method", *Steel Compos. Struct., Int. J.*, **5**(2-3), 203-233.
- Donahey, R.C. and Darwin, D. (1986), "Performance and Design of Composite Beams with Web Openings", SM Report No 18; University of Kansas Centre for Research, USA.
- Durif, S., Bouchair, A. and Bacconnet, C. (2015), "Elastic rotational restraint of web-post in cellular beams with sinusoidal openings", *Steel Compos. Struct., Int. J.*, **18**(2), 325-344.
- Ellobody, E. and Young, B. (2006), "Performance of shear connection in composite beams with profiled steel sheeting", *J. Constr. Steel Res.*, **62**(7), 682-694.
- Erdal, F. (2015), "The comparative analysis of optimal designed web expanded beams via improved harmony search method", *Struct. Eng. Mech., Int. J.*, **54**(4), 665-691.
- Erdal, F. (2016), "Effect of stiffeners on failure analyses of optimally designed perforated steel beams", *Steel Compos. Struct., Int. J.*, **22**(1), 183-201.
- Gattesco, N. (1999), "Analytical modelling of nonlinear behaviour of composite beams with deformable connection", *J. Constr. Steel Res.*, **52**(2), 195-218.
- Kataoka, M.N., Friedrich, J.T. and El Debs, A.H.C. (2017), "Experimental investigation of longitudinal shear behavior for composite floor slab", *Steel Compos. Struct., Int. J.*, **23**(3), 351-362.
- Ko, C. (2002), "A unified approach for steel and composite beams with web openings", Ph.D. Dissertations; Hong Kong Polytechnic University, Hong Kong.
- Lawson, R.M. (2011), Design of Composite Beams with Web Openings, The Steel Construction Institute Publication 355.
- Lawson, R.M., Lim, J., Hicks, S.J. and Simms, I. (2006), "Design of composite asymmetric cellular beams and beams with large web openings", *J. Constr. Steel Res.*, **62**(6), 614-629.
- Lawson, R.M., Lim, J.B.P. and Popo-Ola, S.O. (2013), "Pull-out forces in shear connectors in composite beams with large web openings", *J. Constr. Steel Res.*, **87**, 48-59.
- Lin, Z., Liu, Y. and He, J. (2014), "Behavior of stud connectors under combined shear and tension loads", *Eng. Struct.*, **81**, 362-376.
- Liu, T.C.H. and Chung, K.F. (2003), "Steel beams with large web openings of various shapes and sizes: finite element investigation", *J. Constr. Steel Res.*, **59**(9), 1159-1176.
- Mirza, O. and Uy, B. (2010), "Effects of the combination of axial and shear loading on the behaviour of headed stud steel anchors", *Eng. Struct.*, **32**(1), 93-105.
- Nguyen, H.T. and Kim, S.E. (2009), "Finite element modeling of push-out tests for large stud shear connectors", *J. Constr. Steel Res.*, **65**(10-11), 1909-1920.
- Panedpojaman, P. and Thepchatri, T. (2013), "Finite element investigation on deflection of cellular beams with various configurations", *Int. J. Steel Struct.*, **13**(3), 487-494.
- Panedpojaman, P., Thepchatri, T. and Limkatanyu, S. (2014), "Novel design equations for shear strength of local web-post buckling in cellular beams", *Thin-Wall Struct.*, **76**, 92-104.
- Panedpojaman, P., Thepchatri, T. and Limkatanyu, S. (2015), "Novel simplified equations for Vierendeel design of beams with (elongated) circular openings", *J. Constr. Steel Res.*, **112**, 10-21.
- Panedpojaman, P., Sae-Long, W. and Chub-uppakarn, T. (2016), "Cellular beam design for resistance to inelastic lateral-torsional buckling", *Thin-Wall Struct.*, **99**, 182-194.
- Serror, M.H., Hamed, A.N. and Mourad, S.A. (2016), "Numerical study on buckling of steel web plates with openings", *Steel Compos. Struct., Int. J.*, **22**(6), 1417-1443.
- Sheehan, T., Dai, X., Lam, D., Aggelopoulos, E., Lawson, M. and Obiala, R. (2016), "Experimental study on long spanning composite cellular beam under flexure and shear", *J. Constr. Steel Res.*, **116**, 40-54.
- Wang, A.J. and Chung, K.F. (2008), "Advanced finite element modelling of perforated composite beams with flexible shear connectors", *Eng. Struct.*, **30**(10), 2724-2738.
- Ward, J.K. (1990), Design of Composite and Non-composite Cellular Beams, The Steel Construction Institute Publication 100.

CC